

A QUESTION OF MASS : ACCOUNTING FOR ALL THE DUST IN THE CRAB NEBULA WITH THE DEEPEST FAR INFRARED MAPS

J. Matar¹, C. Nehm ^{1,2} and M. Sauvage²

Abstract. Supernovae represent significant sources of dust in the interstellar medium. In this work, deep far-infrared (FIR) observations of the Crab Nebula are studied to provide a new and reliable constraint on the amount of dust present in this supernova remnant. Deep exposures between 70 and 500 μm taken by PACS and SPIRE instruments on-board the Herschel Space Telescope, compiling all observations of the nebula including PACS observing mode calibration, are refined using advanced processing techniques, thus providing the most accurate data ever generated by Herschel on the object. We carefully find the intrinsic flux of each image by masking the source and creating a 2D polynomial fit to deduce the background emission. After subtracting the estimated non-thermal synchrotron component, two modified blackbodies were found to best fit the remaining infrared continuum, the cold component with $T_c = 8.3 \pm 3.0$ K and $M_d = 0.27 \pm 0.05 M_\odot$ and the warmer component with $T_w = 27.2 \pm 1.3$ K and $M_d = (1.3 \pm 0.4) \times 10^{-3} M_\odot$.

Keywords: *Dust, Supernova Remnant, Crab Nebula, FIR, SED, Herschel, Synchrotron.*

1 Introduction

It is well established that dust is efficiently formed in regions around asymptotic giant branch (AGB) stars. Thus AGB stars are classically considered as the primary source of dust grains in galaxies. Nevertheless, they cannot inject enough dust in the interstellar medium to compensate for the known destruction rates. Supernova (SN) explosions in the interstellar medium (ISM) trigger shock waves that are considered the dominant mechanism of dust destruction. Yet there is increasing evidence for the formation of non-negligible quantities of dust grains in the ejecta of SNe (Bocchio et al. 2016). The Spitzer and Herschel space telescopes have thus observed supernovae remnants (SNRs), currently known to be major sources of dust. Such is the case of the Crab Nebula, a young, bright and well resolved SN at a distance of 2 kpc (Trimble 1973), where large amounts of dust have been reported. Unlike other remnants, there is almost no interstellar material in front of or behind the Crab Nebula, so the possibility that the observed dust is simply the local ISM swept up by the expanding shockwave is disfavoured. Therefore, it represents an ideal case for deriving the total dust mass produced by a SNR. Previous studies using Herschel deduced masses ranging between 0.12-0.25 M_\odot (Gomez et al. 2012) and 0.019-0.13 M_\odot (Temim & Dwek 2013). These results consistently indicate that dust is formed in the ejecta, but their variability shows that much work is still needed to get a reliable estimate of the dust yields by SN. We also note that the Crab Nebula is ionized by non-thermal radiation (MacAlpine & Satterfield 2008) thus measuring accurately the synchrotron emission is important to correctly derive the dust thermal emission.

2 Observations

The Crab Nebula was observed using Herschel (Pilbratt et al. 2010) between September 2009 and September 2010. The PACS (Poglitsch et al. 2010) and SPIRE (Griffin et al. 2010) instruments performed photometry (Figure 1) at 70, 100, 160, 250, 350 and 500 μm (see Table 1). The PACS data were first reduced using HIPE, the Herschel Interactive Processing Environment (Ott 2010). Then the “unimap” software (Piazzo et al. 2015), a generalized least-squares map maker for Herschel data, was used to get rid of low frequency noise in the maps.

¹ Department of Physics & Astronomy, Notre Dame University, Lebanon; cnehme@ndu.edu.lb

² Laboratoire AIM, CEA/IRFU/Dep. d’Astrophysique, CNRS, Universit  Paris Diderot, 91191 Gif-sur-Yvette, France

All PACS observations were combined in one map per photometer band. For SPIRE, the standard pipeline HIPE version 14.0.0 was used (Griffin et al. 2010). Note that in this study, we have included for the first time data that was obtained on the Crab Nebula during the testing and qualification of PACS observing modes, thus nearly doubling the depth of the resulting maps.

Table 1. Photometric observations of the Crab Nebula using Herschel Space Observatory.

Obs. ID	Obs. Date	Obs. Duration (s)	Instrument	Filter set λ (μm)
1342183905	2009-09-15	2221	PACS	(70, 160)
1342183906	2009-09-15	2221	PACS	(70, 160)
1342183907	2009-09-15	2221	PACS	(70, 160)
1342183908	2009-09-15	2221	PACS	(70, 160)
1342183909	2009-09-15	2221	PACS	(100, 160)
1342183910	2009-09-15	2221	PACS	(100, 160)
1342183911	2009-09-15	2221	PACS	(100, 160)
1342183912	2009-09-15	2221	PACS	(100, 160)
1342191181	2010-02-25	4555	SPIRE	(250, 350, 500)
1342204441	2010-09-13	1671	PACS	(70, 160)
1342204442	2010-09-13	1671	PACS	(100, 160)
1342204443	2010-09-13	1671	PACS	(70, 160)
1342204444	2010-09-13	1671	PACS	(100, 160)

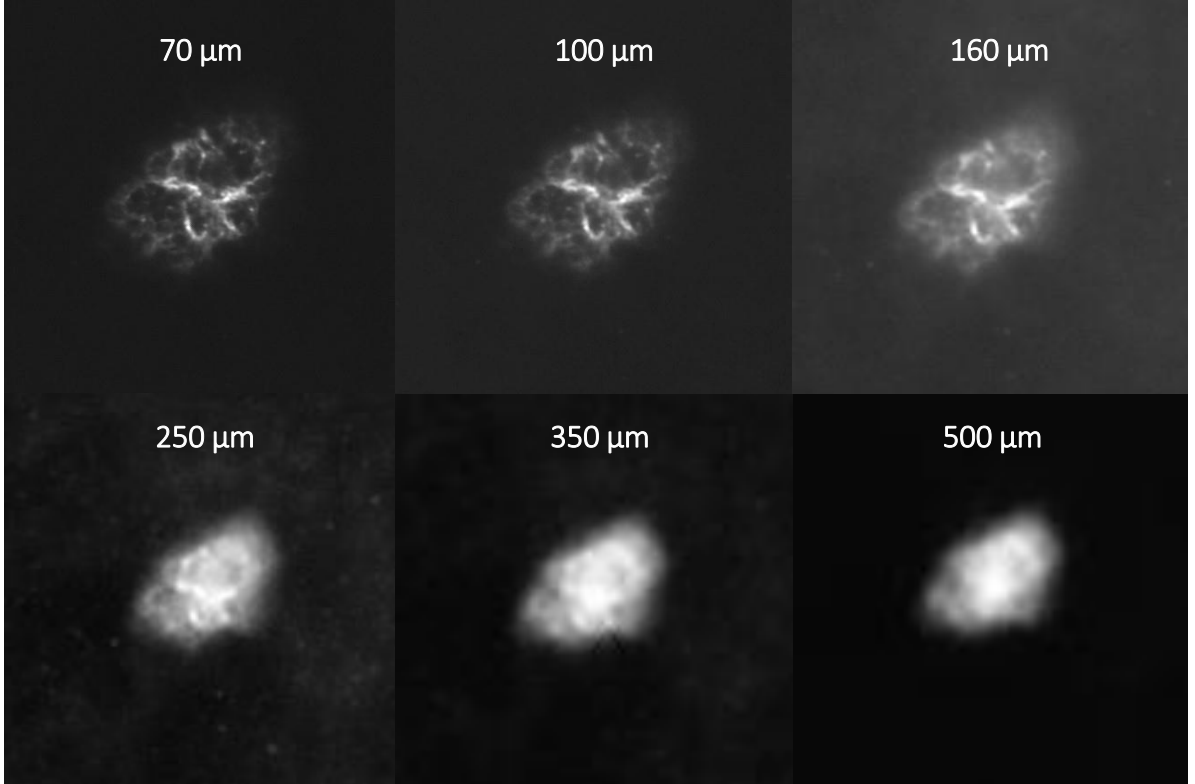


Fig. 1. *Top:* Herschel PACS 70, 100 and 160 μm images. *Bottom:* Herschel SPIRE 250, 350 and 500 μm images.

3 Analysis

3.1 Aperture Photometry and Background Subtraction

To build the overall SED of the Crab Nebula, we performed aperture photometry on the maps. We defined a single aperture that contains the full extent of the Crab Nebula at all observed wavelengths. Since the apparent size of an object increases with the wavelength when observed with the same telescope, we define the aperture on the longest wavelength image, the 500 μm map. The same circular aperture was used for the six images. In the infrared, there is always more emission than simply the objects we are interested in. Any pixel inside the aperture will see flux from the object and flux from the background. Therefore, we need to estimate the background level and subtract it. For that purpose, we designed a 2D Polynomial Fit Model to estimate the background from the emission outside the circular aperture.

3.2 Synchrotron Emission

The Crab Pulsar B0531+21 is the strongest source of synchrotron radiation in the Galaxy. We estimated the non-thermal synchrotron component by applying a least-squares fit to the Herschel (our data), Spitzer, WISE and Planck data from (Gomez et al. 2012). This produces a power law with a spectral index $\alpha = 0.413 \pm 0.085$.

4 Results

4.1 Flux Determination

In table 2, we list the fluxes extracted from our maps using the analysis method presented above.

Table 2. The background and synchrotron contribution to the fluxes.

λ (μm)	S_{Total} (Jy)	$S_{Background}$ (Jy)	$S_{Synchrotron}$ (Jy)	S_ν (Jy)	ΔS_ν (Jy)
70 μm	220.696	2.523	45.719	172.454	0.186
100 μm	225.227	5.189	52.992	167.047	0.178
160 μm	153.456	28.014	64.369	61.073	0.349
250 μm	214.253	104.637	77.427	32.189	0.217
350 μm	170.179	66.038	88.995	15.147	0.214
500 μm	133.745	29.172	103.15	1.423	0.129

Notes. S_ν is the total dust emission and ΔS_ν is the photometric error due to background subtraction.

4.2 Spectral Energy Distribution

If all dust grains were to share the same size and composition (Bianchi 2013), the emission of the Crab would be that of a modified blackbody (MBB), i.e. a blackbody multiplied by the dust absorption cross section. We use here this simplified approach to model the excess thermal emission observed in the FIR (Figure 2), by the sum of two modified blackbodies identified with a warm and a cold component. The figure shows that the Spitzer and WISE fluxes, consistent with one another, are not reproduced by our fit. This is expected as our model does not represent very small grains able to reach, transiently, very high temperature. We defer this to future work where we will implement a more complex representation of the dust. For all the other data points, the agreement is excellent, and the best-fitting temperatures are shown in Table 3.

4.3 Total Dust Mass

From Laor & Draine (1993) and Weingartner & Draine (2001), the dust mass for each component is:

$$M_d = \frac{S_\nu D^2}{\kappa_\nu B(\nu, T)} \quad (4.1)$$

where, S_ν is the flux density, D is the distance (Earth-Crab Nebula), $B(\nu, T)$ is the Planck function and κ_ν is the dust mass absorption coefficient.

Fig. 2. SED of the Crab Nebula from the IR-radio including Herschel (red points) and Spitzer (black), WISE (purple) photometry and Planck fluxes (Planck Collaboration 2011, blue points). The black line is the total flux obtained from summing the synchrotron and the MBB.

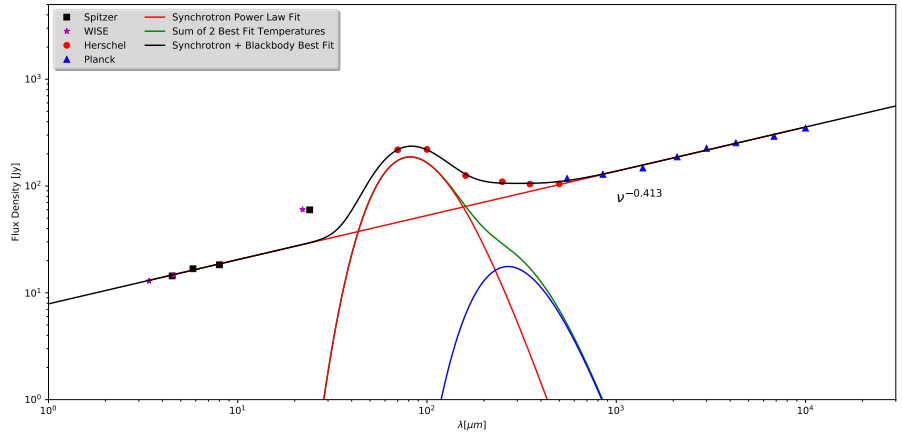


Table 3. Result from the two-component modified black-body fit

Component	Temperature (K)	Mass (M_{\odot})
Warm	27.3 ± 1.3	$(1.3 \pm 0.4) \times 10^{-3}$
Cold	8.2 ± 3.0	0.27 ± 0.05

5 Conclusion

In this work we present maps of the Crab Nebula with double the depth of previous PACS maps. We rederived the mass of dust using a modified black body with two temperature components fitted to the global SED. We report masses of $M_d(\text{cold}) = 0.27 \pm 0.05 M_{\odot}$, $M_d(\text{warm}) = 1.3 \pm 0.4 \times 10^{-3} M_{\odot}$. Our results represent additional support to theoretical models predicting a total dust mass between 0.2 and 0.5 M_{\odot} (Woosley & Weaver (1995) ; Limongi & Chieffi (2003)). Todini & Ferrara (2001) also predict between 0.1 and 0.3 M_{\odot} of dust should form in the ejecta from the (Type-IIP) explosions of progenitor stars with initial mass $< 15 M_{\odot}$ such as the Crab progenitor. Nevertheless, this work is a first step of a long term project that we started on dust in the Crab nebula, to better account for the actual complexity of the source (i.e: filaments) by using the spatial information as well as the spectral information.

Acknowledgement

Dott. Elias Kammoun ... Thank you!

References

- Bianchi, S. 2013, A&A, 552, A89
 Bocchio, M., Marassi, S., Schneider, R., et al. 2016, A&A, 587, A157
 Gomez, H. L., Krause, O., Barlow, M. J., et al. 2012, ApJ, 760, 96
 Griffin, M. J., Abergel, A., Abreu, A., et al. 2010, A&A, 518, L3
 Laor, A. & Draine, B. T. 1993, ApJ, 402, 441
 Limongi, M. & Chieffi, A. 2003, ApJ, 592, 404
 MacAlpine, G. M. & Satterfield, T. J. 2008, AJ, 136, 2152
 Ott, S. 2010, in Astronomical Society of the Pacific Conference Series, Vol. 434, Astronomical Data Analysis Software and Systems XIX, ed. Y. Mizumoto, K.-I. Morita, & M. Ohishi, 139
 Piazzi, L., Calzoletti, L., Faustini, F., et al. 2015, MNRAS, 447, 1471
 Pilbratt, G. L., Riedinger, J. R., Passvogel, T., et al. 2010, A&A, 518, L1
 Poglitsch, A., Waelkens, C., Geis, N., et al. 2010, A&A, 518, L2
 Temim, T. & Dwek, E. 2013, ApJ, 774, 8
 Todini, P. & Ferrara, A. 2001, MNRAS, 325, 726
 Trimble, V. 1973, PASP, 85, 579
 Weingartner, J. C. & Draine, B. T. 2001, ApJ, 548, 296
 Woosley, S. E. & Weaver, T. A. 1995, ApJS, 101, 181